Near Surface Geophysics, 2011, **9**, xxx-xxx doi:10.3997/1873-0604.2010062

The effect of pore size and magnetic susceptibility on the surface NMR relaxation parameter T_2^*

Elliot Grunewald* and Rosemary Knight

Department of Geophysics, Stanford University, 397 Panama Mall, Stanford, CA 94305, USA

Received December 2009, revision accepted October 2010

ABSTRACT

Surface nuclear magnetic resonance (NMR) is a non-invasive geophysical method that can provide valuable information about aquifer properties related to groundwater flow and storage. Our ability to extract such information from surface NMR data, however, is limited by an insufficient understanding of the relaxation parameter T_2^* governing the decay rate of the surface NMR signal in Earth's magnetic field. In this study, we use a combination of numerical and laboratory experiments to systematically explore the effect of two key geologic properties, pore size and magnetic susceptibility, on the T_2^* relaxation process. A one-dimensional numerical model is developed and parametrized to simulate the surface NMR response for a wide range of geologic materials. These simulations illuminate the processes controlling T_2^* relaxation and identify conditions under which T_2^* exhibits varied sensitivity to pore size. For materials with low magnetic susceptibility, T_2^* is highly sensitive to pore size; however, as susceptibility increases, this sensitivity diminishes and T_2^* becomes dominated by complex dephasing effects, particularly when pores are large. Laboratory Earth's field NMR experiments complement the numerical simulations. Measurements on water-saturated quartz sands show that for weakly magnetic materials, T_2^* can be sensitive to pore size and thus could provide useful information about aquifer properties.

INTRODUCTION

Proton nuclear magnetic resonance (NMR) has been used in the Earths sciences since the 1960s, in both laboratory and borehole measurements, as a means of characterizing the pore-scale properties of fluid-saturated geologic media. NMR is ideally suited for this purpose due to a strong link between the measured relaxation parameters T_1 and T_2 and the physio-chemical environment of hydrogen nuclei in the pore fluid. Numerous theoretical and empirical studies have demonstrated robust relationships between these relaxation parameters and geologic properties governing fluid flow and storage, such as pore size (e.g., Gallegos *et al.* 1987; Kenyon *et al.* 1989) and permeability (e.g., Timur 1969; Kenyon *et al.* 1988; Straley *et al.* 1997). Hence, NMR has proven to be a particularly useful well-logging tool in oil and gas applications.

Over the last two decades, new surface-based NMR systems have been developed to extend NMR methods to shallow hydrogeologic applications (Semenov 1987; Legchenko and Valla 2002; Walsh 2008). These systems yield valuable non-invasive NMR relaxation measurements of groundwater to depths of 100 m. Unlike advanced borehole or laboratory NMR methods, which measure T_1 and T_2, standard surface NMR methods directly measure a related, but not equivalent, relaxation parameter T_2^*. Methodologies for approximating T_1 and T_2 with surface NMR have been explored (Legchenko *et al.* 2002; Hertrich 2008), however, the signal measured by surface NMR is fundamentally controlled by T_2^* and it is this relaxation parameter that can be most robustly determined as a function of depth.

The T_2^* relaxation process measured by surface NMR is similar to T_1 and T_2 relaxation, in that it is partially controlled by the pore-scale environment of the groundwater under investigation. However, there is not a simple scaling relationship between T_2^* and T_1 or T_2, and the link between T_2^* and pore-scale properties is not well-understood. This gap in understanding hampers our ability to extract useful information about aquifer properties from surface NMR data. Further, it limits the extent to which we can predict the performance and reliability of surface NMR data in varied geologic environments.

In contrast to the extensive history of T_1 and T_2 research, there have been very few studies of the relationship between T_2^* and pore-scale properties. Several studies have attempted to substitute T_2^* in the petrophysical relationships originally developed for T_1 and T_2, with mixed success (e.g., Legchenko *et al.* 2002; Lubczynski and Roy 2003). Only one study to date has directly explored the relationship between these various relaxation times using laboratory measurements (Müller *et al.* 2005). Further systematic studies of this type are needed to improve our fundamental understanding of the T_2^* response in groundwater aquifers and our ability to effectively interpret these measurements.

* elliotg@stanford.edu

In this study, we use a combination of numerical modelling and laboratory measurements to systematically explore the factors controlling T_2^* relaxation. We begin by developing a pore-scale numerical model to simulate the T_2^* relaxation response measured by surface NMR. Using this model, we vary parameters describing pore size and magnetic susceptibility in order to investigate the T_2^* response for systems representing a range of realistic geologic conditions. Our simulations allow us to illuminate the processes controlling T_2^* relaxation and to identify regimes in which T_2^* exhibits varied sensitivity to the geologic properties of interest. Finally, we present complementary laboratory measurements for a group of natural sands representing a subset class of the modelled systems and find good agreement between the laboratory data and predictions from our numerical modelling. This study provides new insights into the link between T_2^* and geologic properties, required to advance the use of surface NMR in hydrogeologic applications.

BACKGROUND

The NMR signal is observed when nuclear magnetic spins, associated with hydrogen nuclei in a fluid, are perturbed from an equilibrium alignment with a background magnetic field. At equilibrium with the background field B_0, the spins are weakly polarized yielding a net magnetization directed parallel to B_0 (along the z-axis). This magnetization will precess about B_0 at the Larmor frequency, f_0, given by

$$f_0 = \frac{\gamma}{2\pi}|B0|, \tag{1}$$

where γ is the gyromagnetic ratio of hydrogen, equal to 0.2675 rad/(nT/s). For borehole and laboratory NMR measurements, the background field is generated by magnets and f_0 is typically around 2 MHz; for surface NMR measurements, the background field is provided by Earth's magnetic field and f_0 typically ranges between 0.8–2.8 kHz.

In this equilibrium state, the nuclear magnetization cannot be directly observed. To obtain an NMR measurement, an excitation coil is used to pulse the system with a weak secondary field B_1, oscillating at f_0 and applied in the transverse (xy) plane. This excitation pulse rotates the magnetization into the transverse plane, where continued coherent precession of the spins about B_0 generates a detectable signal resonating at f_0. Immediately following excitation, the transverse magnetization begins to decay as spins relax and return to their equilibrium state. As a result, the transverse magnetization signal is enveloped by a decaying function $E(t)$. Depending on the details of the NMR measurement, this decay is characterized by one of two relaxation times: T_2 or T_2^*.

Relaxation in a uniform magnetic field

In the idealized case of a uniform magnetic field, both relaxation times T_2 and T_2^* (or rates T_2^{-1} and T_2^{*-1}) are equivalent. For water saturating a single pore, the decay envelope $E(t)$ is given by

$$E(t) = E_0 e^{-t/T_2}, \tag{2}$$

where the initial decay amplitude, E_0, is proportional to the saturated pore volume. For the commonly assumed condition of fast-diffusion (Brownstein and Tarr 1979), the net observed relaxation rate represents two relaxation processes acting in parallel within the bulk water and at the pore surface:

$$\tilde{T}_2^{-1} = T_{2B}^{-1} + \rho_2 S/V. \tag{3}$$

Here the twiddle on T_2^{-1} signifies the assumption of a uniform field; T_{2B}^{-1} is the relaxation rate of the bulk fluid in a uniform field, S/V is the surface-area-to-volume ratio of the pore (inversely proportional to the pore dimension for simple pore geometries) and ρ_2 is the surface relaxivity, a property describing the capacity of the mineral surface to enhance relaxation. Together, the term $\rho_2 S/V$ is called the surface relaxation rate (denoted sometimes as T_{2S}^{-1}) and provides the link between relaxation times and pore geometry utilized in geophysical applications of NMR to estimate pore size and permeability.

Relaxation in a non-uniform magnetic field

In the case of a non-uniform background magnetic field, an additional relaxation process arises that complicates equation (3). Spatially inhomogeneous magnetic fields may be caused by gradients in the regional/local field or by secondary internal fields induced by magnetic susceptibility contrasts between the grain and fluid. In the presence of a spatially variable background field, spins at different positions in the pore space will precess at slightly different Larmor frequencies (see equation (1)). As a result, the spins will dephase from one another over time and a loss of phase coherence will lead to a more rapid decay of the magnetization signal. This process of dephasing affects T_2 and T_2^* very differently.

In general, T_2 is only weakly affected by dephasing in inhomogeneous fields. This is because refined laboratory or borehole measurements of T_2 use pulse sequencing techniques to periodically refocus the NMR signal and thus mitigate the influence of dephasing (see Dunn *et al.* 2002). The effectiveness of this refocusing, however, can be partly reduced by molecular diffusion, so that some loss of phase coherence will be unrecoverable. Therefore, the complete expression for T_2 contains a third term, T_{2D}^{-1}, known as the diffusion relaxation rate, which acts in parallel with bulk and surface relaxation:

$$T_2^{-1} = T_{2B}^{-1} + \rho_2 S/V + T_{2D}^{-1}. \tag{4}$$

The magnitude of T_{2D}^{-1} is generally proportional to the square of the echo-time t_E, an adjustable parameter of the CPMG pulse sequence (Carr and Purcell 1954). Thus, by using a very short t_E, the effect of magnetic inhomogeneity entering through the T_{2D}^{-1} term can be dramatically reduced or effectively negated in many geologic materials. In the case of a very short echo-time, T_2^{-1} becomes approximately equivalent to T_2^{*-1} and can be interpreted to obtain information about pore-scale properties.

Unlike borehole and laboratory instruments, the standard SNMR method does not use a CPMG pulse sequence and instead measures the so-called free induction decay (FID) signal. The relaxation rate of the FID is much more strongly influenced by the presence of an inhomogeneous field because dephasing is allowed to proceed without mitigation by refocusing pulses. The FID envelope is typically modelled as an exponential decay having a net relaxation rate T_2^{*-1}. The expression for T_2^{*-1} is similar to the expression for T_2^{-1} but includes a term to account for the large effect of dephasing in the absence of refocusing pulses. In this study, we represent this effect using the term $T_{2\mathrm{IH}}^{-1}$, referred to as the inhomogeneous field dephasing rate and express T_2^{*-1} as

$$T_2^{*-1} = T_{2B}^{-1} + \rho_2 S/V + T_{2IH}^{-1} = \tilde{T}_2^{-1} + T_{2IH}^{-1}. \quad (5)$$

In this expression, the term $T_{2\mathrm{IH}}^{-1}$ encompasses all effects related to dephasing in the inhomogeneous field, including any influence diffusion may have on this process.

While equation (5) offers a closed expression for T_2^{*-1}, the presence of the dephasing term complicates the link to pore-scale properties. Additionally, the factors controlling the magnitude of $T_{2\mathrm{IH}}^{-1}$ are not well established. Often, $T_{2\mathrm{IH}}^{-1}$ is approximated as

$$T_{2IH}^{-1} \approx \frac{\gamma}{2\pi}\Delta B, \quad (6)$$

where ΔB is the total variation in the inhomogeneous field (e.g., Chen *et al.* 2003; Müller *et al.* 2005). This simplistic expression, however, cannot be used to directly predict the magnitude of $T_{2\mathrm{IH}}^{-1}$ in geologic materials. Such an expression fails to relate the statistics of the internal inhomogeneous field to quantifiable magnetic properties of the solid and fluid phases. Further, this static approximation implicitly assumes that spins are stationary and does not account for the influence of molecular diffusion.

Neglecting these complications, T_2^* is often treated as a proxy for T_2 in the interpretation of surface NMR data and is used in a similar manner to estimate pore size and permeability (Schirov *et al.* 1991; Yaramanci *et al.* 1999; Legchenko *et al.* 2002). This simplification is made under the assumption that the dephasing term is negligible, either because grains are weakly magnetic or because inhomogeneous fields induced by magnetic grains will not be strong in the presence of Earth's weak background field.

Numerous field calibration and case studies, however, have found that T_2^* is frequently much shorter than anticipated values of T_2 and can be a less robust indicator of pore size and permeability (Vouillamoz *et al.* 2002; Plata and Rubio 2008; Roy *et al.* 2008). In the only published study to date comparing laboratory measurements of T_2 to field surface NMR measurements of T_2^*, Müller *et al.* (2005) clearly demonstrated that T_2 and T_2^* are not always equal. These authors further suggested that the ratio T_2: T_2^* might even be grain-size dependent, increasing from ~1:1 in fine sand to ~3:1 in gravel. Clearly, an improved understanding of the factors controlling T_2^* and the measured FID signal is required to advance the use of surface NMR as a technique for characterizing groundwater aquifers.

In order to most effectively inform the interpretation of surface NMR data, relaxation processes must be systematically studied under conditions that are analogous to surface NMR measurements. In particular, because the magnitude of inhomogeneous fields and thus the T_2^* relaxation rate are strongly dependent on the background magnetic field, the FID response must be probed under Earth's field conditions, rather than under higher field conditions typically utilized in laboratory or borehole applications. In this study, we take advantage of flexible numerical simulation algorithms and recently developed laboratory instruments to directly explore the factors influencing the Earth's field T_2^* relaxation response, as measured in hydrogeologic applications of surface NMR.

NUMERICAL MODELING

Several previous studies have illustrated the value of numerical modelling using random walk methods to explore the pore-scale controls on NMR relaxation measurements (e.g., Mendelson 1993; Valckenborg 2002). These methods are highly flexible and can be adapted to model multiple relaxation processes for arbitrary pore models, magnetic fields and pulse sequencing schemes. Here, we develop a random walk algorithm that simulates the NMR free induction decay in Earth's magnetic field, as measured by surface NMR methods. These simulations allow us to investigate how the relevant T_2^* decay process will vary across a wide range of geologic materials.

Numerical simulations

For our numerical simulations, we consider a one-dimensional pore model in which an inhomogeneous field is induced by magnetic grains. We parametrize the pore model to be representative of varied geologic materials. For each parametrized model, we use a random walk algorithm to fully simulate the coupled processes of molecular diffusion, surface relaxation and dephasing. We first describe the parametrization of the model space and internal fields and then describe our random-walk algorithm.

The one-dimensional pore model, of radius r_p is bounded on either side by a grain with volume magnetic susceptibility χ_g and surface relaxivity ρ_g; the saturating pore fluid has susceptibility χ_f and self-diffusion coefficient D_f. A background magnetic field of magnitude B_0 and susceptibility contrast between the grain and fluid $\delta\chi = |\chi_g - \chi_f|$ induces a secondary, internal magnetic field H, which is spatially variable. Only the component of the secondary field that is parallel to B_0 influences relaxation; we hereafter use H to refer only to this parallel component.

The statistics of H inside the pore are modelled after studies by Song (2003) and Audoly *et al.* (2003). These authors directly simulated the internal magnetic field distribution arising in a random pack of magnetic spheres. They demonstrated that variation in the internal field occurs primarily within individual pores and that the field is statistically similar between pores; therefore, it is meaningful to consider relaxation in a single pore for this study. Audoly *et*

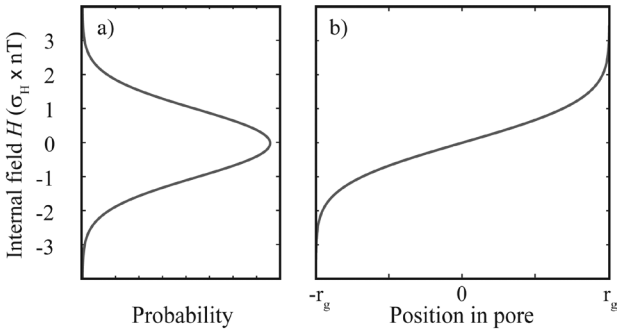

FIGURE 1

Statistical distribution of the internal magnetic field H in the 1D pore model. a) The probability distribution of H within the pore is Gaussian; units on the y-axis are in unit increments of the standard deviation of σ_H. b) The spatial profile of H within the pore is plotted as a function of the position in the pore.

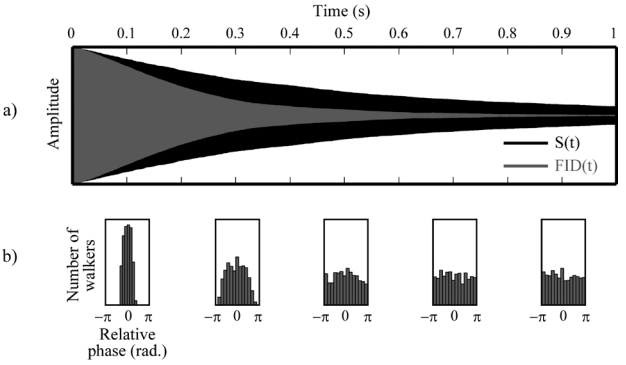

FIGURE 2

An example numerical simulation for one parametrized pore model. a) The signal *S(t)* in black models bulk-fluid and surface relaxation; the simulated signal *FID(t)* in grey additionally models dephasing effects. b) Time stepped histograms show the relative phase for the ensemble of walkers at 0.2 s intervals.

al. (2003) further found that the magnitude and profile of the internal field is independent of pore or grain size and has a probability density function (pdf) with zero-mean with a second moment σ_H given by $0.642(4\pi)\delta\chi B_0/3$. We thus approximate the pdf of H as Gaussian, $H \sim N(0, \sigma_H^2)$. The spatial profile of the field, $H(x)$, increases from a minimum at the left pore wall, through a zero-crossing in the centre of the pore, to a maximum at the right pore wall. In Fig. 1, we illustrate this probability distribution (a) and spatial distribution (b) of H used in the parametrized pore model.

Within this parametrized model space, we simulate relaxation using a random walk algorithm modified from Mendelson (1993) and Valckenborg *et al.* (2002). We populate the 1D pore space with n walkers, which simulate discrete packets of diffusing spins with nuclear magnetization. For each i^{th} walker, we track three properties over the course of a simulation: position $x_i(t)$; phase $\phi_i(t)$; and a binary state $\psi_i(t)$ describing whether the walker is active ($\psi_i = 1$) or has relaxed ($\psi_i = 0$).

At time-zero, we distribute all walkers uniformly throughout the pore space with zero phase and in an active state. These initial conditions describe the system immediately following the excitation pulse when the transverse magnetization is maximum and spatially uniform. At each subsequent time step of spacing Δt, we update x_i, ϕ_i, and ψ_i for each walker to simulate dephasing, diffusion and surface relaxation.

We first update the walker phase. At every time step, each walker accumulates an incremental phase shift determined by the magnetic field at its current position (Valckenborg *et al.* 2002):

$$\Delta\phi_i = \gamma\left(B_0 + H\left(x_i\right)\right)\Delta t. \tag{7}$$

This incremental phase shift is added to the walker phase from the previous time step to yield an updated value of the total accumulated phase ϕ_i at the new time step. Because walkers at different locations within the pore model experience a different internal field $H(x)$, they will accumulate different phase shifts and thus will dephase from one another over time.

Following the phase update step, we update the walker position by random walk to simulate molecular diffusion. Each walker moves from its previous position, with equal probability to the left or right, by a distance

$$\Delta x = \pm\sqrt{2D_f\Delta t}, \tag{8}$$

to an updated position. At this point, we also incorporate the process of surface relaxation. If the walker's new position falls outside of the pore space, the walker relaxes with a probability α, which is proportional to ρ_g (Mendelson 1993):

$$\alpha = \frac{\rho_g \Delta x}{D_f}. \tag{9}$$

If the walker does not relax, it reflects back into the pore space. It is important to note that after diffusing to a new position, any given walker will experience a slightly different magnetic field at the next time step and thus a different phase shift.

After all walkers have been updated in a time step, we calculate two signals: *S(t)*, which only models bulk-fluid and surface relaxation and *FID(t)*, which additionally models dephasing. These signals are defined as follows:

$$S\left(t\right) = \frac{e^{-t/T_{2B}}}{n}\sum_j \Psi_i\left(t\right)\cos\left(\gamma B_0 t\right), \tag{10}$$

and

$$FID\left(t\right) = \frac{e^{-t/T_{2B}}}{n}\sum_j \Psi_i\left(t\right)\cos\left(\phi_j\left(t\right)\right). \tag{11}$$

We show an example simulation of these two signals in Fig. 2(a); *S(t)* is shown in black and *FID(t)* is shown in grey. Both signals have a centre frequency equal to the Larmor frequency but exhibit different decay rates.

The first signal *S(t)* only includes the two relaxation mechanisms that dominate T_2 in the case of a short echo-time. Bulk-fluid relaxation enters explicitly through multiplication by the bulk-fluid exponential decay. Surface relaxation, on the other hand, is directly modelled by summing over the state variable, which indicates the fraction of walkers that have not yet relaxed at a surface. As modelled here, *S(t)* does not include effects that would be associated with the term T_{2D}^{-1}. We note, however, that for the systems considered in this study, this T_{2D}^{-1} term would be negligible provided the echo-time is short. The second signal *FID(t)* models the complete free induction decay exhibiting T_2^* relaxation. In addition to bulk-fluid and surface relaxation, *FID(t)* additionally simulates dephasing by summing over the in-phase component of each walker. In Fig. 2(b), we show time-stepped histograms of the relative phase for the ensemble of walkers during the simulation. We see that, as the walkers lose phase coherence in the inhomogeneous field over time, *FID(t)* undergoes a more rapid decay than *S(t)*.

For each simulation, we estimate the relaxation rates T_2^{-1} and T_2^* by least-squares fitting of an exponential decay to the envelope of *S(t)* and *FID(t)*, respectively. Using equation (5), we can then take the difference of these rates to obtain a quantitative measure of the inhomogeneous field dephasing rate, T_{2IH}^{-1} , which isolates the additional mechanism affecting T_2^* relaxation.

We apply this approach for a suite of simulations using different parametrized models to explore the sensitivity of the relaxation rates to certain model parameters. We anticipate that pore size, grain susceptibility and surface relaxivity will significantly affect the relaxation behaviour; therefore, we vary χ_g, r_p, and ρ_g over a wide range of values in our simulations. For all simulations, we hold fixed the parameters that describe the pore fluid to be representative of groundwater: χ_{fluid} = -7.190 10^{-6} cgs (Lide 2003), T_{2B}^{-1} = 0.3 s, a lower limit for fresh water (Dunn *et al.* 2002) and D_f = 1.58 10^{-9} m^2/s for water at 15° C (Simpson and Carr 1958). We set B_0 = 50 000 nT, a typical value for the magnitude of Earth's magnetic field at mid-latitudes. For all simulations, we model n = 10 000 walkers; we use a time discretization of $\Delta t = 1/(10 f_0) \sim 50$ µs.

Numerical results

For the discussion of our numerical results, we first focus separately on the dephasing rate, T_{2IH}^{-1}, which characterizes the principle difference between T_2^* and T_2 relaxation. In Fig. 3, we show the estimated dephasing rate for a collection of simulations between which both pore radius and magnetic susceptibility are varied; each simulation result is plotted as a separate point. Along the top x-axis of the log-log plot, pore radius r_p decreases from left to right; along the bottom x-axis, the inverse pore radius r_p^{-1} approximates the pore surface-area-to-volume ratio. Grain susceptibility χ_g is indicated by the colour of each point, with colours warming as χ_g increases. For reference, a χ_g-value of 5 10^{-6} cgs (blue) is typical of quartz; 100 10^{-6} cgs (gold) is typical of pyroxene or pyrite; 2000 10^{-6} cgs (red) is typical of hematite (Hunt *et al.* 1995); cgs units are converted to SI through multiplication by a factor of 4π (i.e., $\chi_g^{SI} = 4\pi\, \chi_g^{CGS}$). The value of T_{2B}^{-1} is shown as a dashed line for reference. Surface relaxivity ρ_g is held fixed at an intermediate value of 30 µm/s.

The results shown in Fig. 3 reveal a dependence of T_{2IH}^{-1} on both χ_g and pore size. For a given pore size, we see that T_{2IH}^{-1} is highly sensitive to χ_g and increases substantially as χ_g increases. This result can be anticipated as higher χ_g will give rise to stronger inhomogeneous internal fields and thus more rapid dephasing. In general, T_{2IH}^{-1} increases linearly with χ_g because the standard deviation of the internal field σ_H scales linearly with χ_g.

The dependence of T_{2IH}^{-1} on the pore size is somewhat more complicated. Consider an intermediate χ_g-value of 100 10^{-6} cgs. We define a critical pore size $r_{p,crit}$ and identify two regions in the data: $r_p > r_{p,crit}$ and $r_p < r_{p,crit}$. In the region of $r_p > r_{p,crit}$, T_{2IH}^{-1} is approximately constant and reaches a maximum value. This maximum value can be roughly approximated as $\gamma\Delta B$ (as in equation (6)) if we take ΔB as the variation in the internal field at two standard deviations (two times σ_H). In the region of $r_p < r_{p,crit}$, T_{2IH}^{-1} displays a power law dependence on r_p ($T_{2IH}^{-1} \sim r_p^{-2}$), decreasing with pore size. We observe similar behaviour over the full range of modelled χ_g-values but note that $r_{p,crit}$ becomes smaller as χ_g increases.

We explain these trends by considering the effects of diffusion in the context of relaxation regimes described by Hurlimann (1998). In the 'localization regime', ($r_p > r_{p,crit}$), which occurs when pores are large or the inhomogeneous internal field is strong, spins entirely dephase before they are able to diffuse across the pore space. As a result, the dephasing rate is insensitive to pore geometry (constant with r_p) and simply reflects the total variation in the magnetic field across the pore. Once pores become small enough that spins can diffuse across the pore space before fully dephasing, we enter the 'motional averaging' regime ($r_p < r_{p,crit}$). In this regime, spins are able to partially average out variations in the zero-mean internal field by diffusion and so dephase less rapidly. As pore size decreases, this averaging process occurs with greater efficiency and the net observed dephasing rate shows a marked decrease with reduced pore size. We note that this tendency for diffusion to decrease the magnitude of T_{2IH}^{-1} in the expression for T_2^{*-1}, contrasts the general tendency for diffusion to increase the magnitude of the term T_{2D}^{-1} in the expression for T_2^{-1}.

In the simulations shown here, ρ_g is held constant. We find that T_{2IH}^{-1} shows only a weak dependence on ρ_g and tends to decrease slightly as ρ_g increases. We explain this effect by recognizing that dephasing occurs most rapidly close to the pore wall where H is strongest; this is also where surface relaxation occurs. Thus, increased ρ_g causes the most rapidly dephasing spins to relax quickly, leaving the remaining spins with a slightly higher average phase coherence. We stress, however, that this sensitivity to ρ_g, is insignificant when compared to the sensitivity to χ_g and r_p.

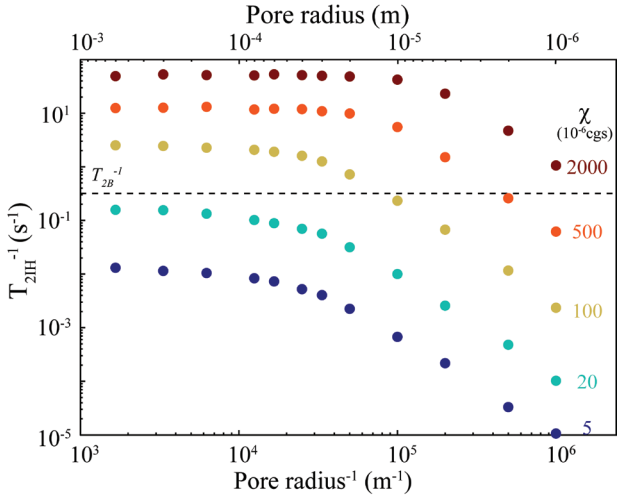

FIGURE 3

Numerically simulated values of the dephasing rate T^{-1}_{2IH} for a collection of parametrized pore models with varied pore radius r_p and grain susceptibility χ_g. Each simulation result is plotted as a point; the parametrized value of χ_g is indicated by the colour of the point, with colours warming as χ_g increases; r_p decreases from left to right along the top axis; along the bottom x-axis r_p^{-1} approximates the pore surface-area-to-volume ratio.

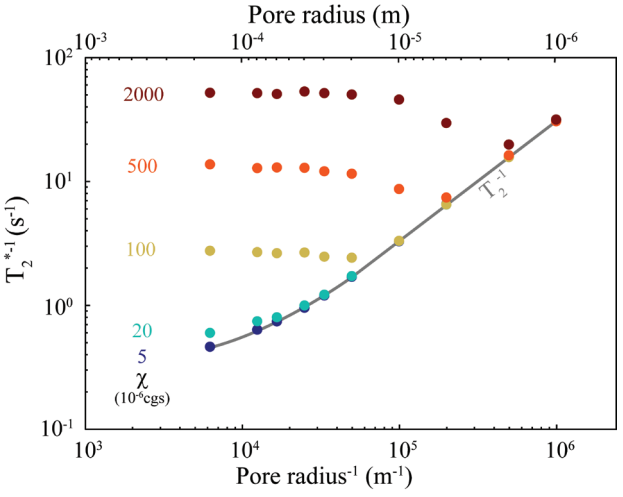

FIGURE 4

Numerically simulated values of T_2^{*-1} for a collection of parametrized pore models with varied pore radius r_p and grain susceptibility χ_g. Each simulation result is plotted as a point; the parametrized value of χ_g is indicated by the colour of the point, with colours warming as χ_g increases; r_p decreases from left to right along the top axis; along the bottom x-axis r_p^{-1} approximates the pore surface-area-to-volume ratio. Simulated values of T_2^{-1} are shown as a grey line.

Thus far, we have illustrated how varied pore size and susceptibility affect the rate of dephasing in an inhomogeneous field. Let us now explore the sensitivity of the full T_2^{*-1} relaxation rate as measured by surface NMR. In Fig. 4, we plot T_2^{*-1} for our suite of simulations, using the same axes and colour scale as previously. We display as a grey line the simulated value of T_2^{-1}.

The trend of T_2^{-1} is dominated by a linear dependence on r_p^{-1}, because there is no contribution from dephasing. We stress this linear dependence on r_p^{-1} (approximating S/V) is required in order to robustly estimate pore size or permeability from measured relaxation times. We observe that when χ_g is very low (blue points), simulated values of T_2^{*-1} closely approximate T_2^{-1}, because the T_{2IH}^{-1} term is negligible and exhibits a similar dependence on r_p^{-1}. For increasing values of χ_g, however, the sensitivity to r_p^{-1} (and agreement between T_2^{*-1} and T_2^{-1}) is only observable over a limited range of smaller pore sizes. For large pores, T_2^{*-1} does not provide a clear link to pore size; in fact, under certain conditions, the trend of T_2^{*-1} with r_p^{-1} is actually inverted, exhibiting faster relaxation in larger pores.

We explain this observed behaviour of T_2^{*-1} at intermediate χ_g by considering results from Fig. 3 in the context of equation (5). When pores are large, the surface relaxation rate $\rho_2 S/V$ is low and the expression for T_2^{*-1} will be dominated by the dephasing rate T_{2IH}^{-1}. As pores become smaller, however, T_{2IH}^{-1} decreases while $\rho_2 S/V$ simultaneously increases and begins to dominate the net relaxation rate. Though not shown here, increasing surface relaxivity slightly increases the range over which the $\rho_2 S/V$-term will dominate and steepens the trend of T_2^{*-1} with r_p^{-1}.

Our numerical results suggest several important implications for the interpretation of surface NMR measurements. First, for low susceptibility materials ($|\chi|$<~10 10^{-6} cgs), we find that T_2^{*-1}, like T_2^{*-1}, provides a reliable indication of pore size and thus might also be used to estimate permeability. For materials with high susceptibility ($|\chi|$>~2000) 10^{-6} cgs, T_2^{*-1} does not clearly reflect pore size; however, we note that T_2^{*-1} always provides an upper bound on T_2^{-1}. For materials with intermediate susceptibility (between these values), T_2^{*-1} measurements only reflect pore size over a limited range of small pore radii; for large pore radii, T_2^{*-1} becomes dominated by dephasing and is primarily sensitive to subtle variations in magnetic properties.

In the context of Fig. 4, we can roughly predict the behaviour of T_2^{*-1} in specific geologic materials. For example, in highly felsic sediments, which may have an average-χ around 10 10^{-6} cgs, we expect that T_2^{*-1} will be dominated by surface relaxation and can provide reliable estimates of pore size and potentially permeability in both coarse and fine sediments. In an intermediate composition sediment that may have an average-χ closer to 100 10^{-6} cgs, T_2^{*-1} will only be sensitive to pore size in fine sands and silts that have a pore radius less than ~50 μm. We note that, although not modelled here, the presence of regional gradients in the local magnetic field will also influence T_{2IH}^{-1} and can reduce the sensitivity of T_2^{*-1} to pore size in certain environments.

Our results in Fig. 4 can additionally be used to identify geological conditions in which standard surface NMR measurements may fail entirely. One fundamental constraint of the surface NMR method is a short recording delay, known as the instrument dead-time, which prevents measurement of the earli-

est portion of the FID signal. We see that when magnetic susceptibility exceeds ~2000 10^{-6} cgs, T_2^{*-1} will be so rapid that little to no signal will be recorded if the dead-time is greater than around 30 ms. If the dead-time is much longer than the decay time, it will be impossible to quantify the decay rate or even to determine the initial signal amplitude, required to estimate water content. Numerical modelling thus provides a useful approach to broadly evaluate the viability of surface NMR as a method for estimating aquifer properties in a range of geologic conditions.

LABORATORY EXPERIMENTS

Our numerical modelling results provide important insights into the factors controlling the T_2^* relaxation response, which we can further evaluate using controlled laboratory experiments. Previously published laboratory studies of T_2^* (Müller *et al.* 2005; Chen *et al.* 2005) have measured the FID response of geologic samples using instruments that impose a strong background magnetic field (at least 0.05 T). Because the magnitude of inhomogeneous fields affecting T_2^* scales with the background field, previously published data are of limited relevance to surface NMR measurements conducted in Earth's field (~0.05 mT). In this study, we take advantage of the recent development of laboratory Earth's field NMR instruments (Callaghan *et al.* 2007), in order to quantify the NMR response of controlled samples under conditions more closely analogous to actual surface NMR measurements.

We describe a series of Earth's field laboratory NMR experiments designed to test specific findings from our numerical results. For the current study, we focus exclusively on low-susceptibility materials and aim to evaluate the finding suggested by our numerical results that, in low-susceptibility materials, Earth's field measurements of T_2^* provide a robust indication of pore size. These experiments represent one of the first attempts to directly assess the T_2^* response of porous media in Earth's field conditions and provide a framework for future laboratory experiments exploring a wider class of materials.

Laboratory materials and methods

We investigate the Earth's field NMR response of a collection of water-saturated quartz sand samples, prepared with varied grain size. All samples are derived from natural quartz sands mined from the St. Peters deposit in Wedron, Ohio, USA and were provided by Fairmount Minerals Ltd, Ohio, USA. These sands have a well-rounded grain shape and a mineral composition that is greater than 99.5% SiO_2.

The original sands were first sieved to isolate twelve samples between which the mean grain radius r_{grain} varies. Values of r_{grain} for each sample, determined by mesh size, are listed in Table 1 and range over an order of magnitude from 32–385 μm. All samples were also processed through a magnetic separator to remove stray magnetic grains and were rinsed with a light acid (5% HCl) to remove powder residues and surface contamination introduced by sieving. Magnetic susceptibility was measured using a Sapphire SI2 Susceptibility Bridge and was found to be less than 5 10^{-6} cgs in magnitude for all samples.

For NMR measurements, we packed dry volumes of each sample by hand into 175 mL cylindrical glass containers (diameter = 5.5 cm) and saturated the samples with deionized water. Estimates of porosity were obtained by weighing the samples both before and after saturation. For all samples, we found that porosity was between 0.39– 0.41 and showed no trend with grain size.

The Earth's field NMR measurements were collected using a

TABLE 1
Tabulated values of r_{grain}, T_2^{*-1} and T_2^{-1} for laboratory Earth's Field NMR measurements on water-saturated quartz sands

	r_{grain} (μm)	T_2^{*-1} (s^{-1})	T_2^{1} (s^{-1})
Water	–	0.769	0.492
Quartz sands	385	2.33	0.909
	325	2.03	0.800
	275	2.25	0.926
	213	3.05	0.971
	151	3.37	1.51
	120	3.61	1.82
	102	3.97	2.22
	82	3.88	2.27
	68	4.63	2.56
	58	4.66	2.78
	45	4.93	3.33
	32	6.96	4.67

Terranova-MRI system (Magritek Ltd). This instrument uses prepolarization and adiabatic switching (Callaghan *et al.* 2007) to increase the NMR signal strength, which is otherwise weak in Earth's field. A strong polarizing magnetic field B_p is applied to the sample for a brief duration (~5 s), generating a strong nuclear magnetization parallel to B_p. The B_p field is then switched off adiabatically (over several ms) allowing the magnetization to realign parallel to the background Earth's field. Standard pulsed NMR experiments then proceed utilizing this enhanced magnetization to generate a detectable Earth's field NMR signal. The instrument also uses three-component gradient coils to shim regional gradients in the background field.

Optimal acquisition parameters, related to tuning, shimming and pulse timing were determined for a sample of bulk pore water and were maintained for all subsequent measurements. For each sample, we recorded the FID signal using the shortest available instrument dead time of 25 ms. All measurements were stacked four times to improve the signal-to-noise ratio. We determine the relaxation rate T_2^{*-1} by least-squares fitting of an exponential decay (with a baseline offset to account for noise) to the envelope of the measured FID signal. For each sample, we also measured T_2^{-1} using a CPMG pulse sequence.

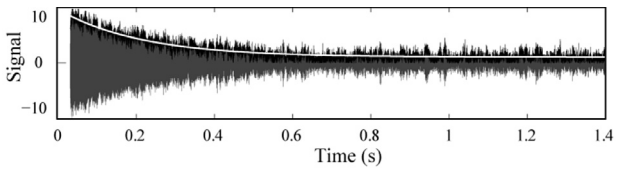

FIGURE 5

An example of an Earth's field NMR measurement of the free induction decay signal for water-saturated quartz sand with a mean grain radius of 58 μm. The recorded signal is plotted in grey; the estimated envelope is plotted in black; the exponential fit is superimposed in white.

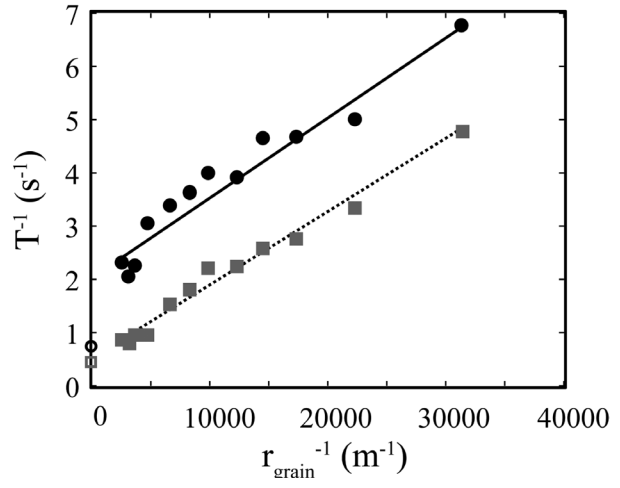

FIGURE 6

Values of T_2^{*-1} (filled black circles) and T_2^{-1} (filled grey squares) for laboratory Earth's field NMR measurements on water-saturated quartz sands with varied mean grain radius; the inverse mean grain radius r_{grain}^{-1} (approximately proportional to the pore surface-area-to-volume ratio) increases along the *x*-axis. The solid line and dashed line are linear fits to the T_2^{*-1} and T_2^{-1} data, respectively. Values of T_2^{*-1} and T_2^{-1} for a sample of bulk pore water are shown as hollow points.

Laboratory results

In Fig. 5, we plot an example FID signal for one of the saturated sand samples (r_{grain} = 58 μm). The recorded signal is plotted in grey, with the envelope plotted in black and the exponential fit overlaid in white. We observe a very good fit to the data and note that the signal-to-noise ratio is approximately 10; this data quality is typical for all our measurements. In Fig. 6, we plot values of T_2^{*-1} for each sample as black circles versus r_{grain}^{-1}, which is approximately proportional to *S/V*; T_2^{*-1} for a sample of the bulk pore water is plotted as an open black circle. All values are also listed in Table 1.

Given that the quartz sands have very low-susceptibility, our numerical simulations predict that T_2^{*-1} should be dominated by a linear dependence on r_{grain}^{-1}. Indeed, the data exhibit a strong trend with r_{grain}^{-1}, which is well fit by a linear relationship (R^2 = 0.94), plotted as a solid black line. This result confirms that for Earth's field measurements in weakly magnetic materials, T_2^{*-1} is dominated by the surface relaxation rate $\rho_2 S/V$ and thus can be used to estimate pore size and potentially permeability.

We note that subtle deviations from the linear trend are apparent in the experimental data. One likely explanation for these deviations is that r_{grain}^{-1} is not an ideal proxy for *S/V* due to the presence of rough grain surfaces. We also observe that the linear trend does not perfectly intersect the *y*-axis at the bulk-fluid relaxation rate, as would be predicted in the absence of dephasing; rather, the *y*-intercept is offset slightly higher.

To further investigate the reason for this offset, we compare values of T_2^{*-1} from FID measurements to values of T_2^{-1} from CPMG measurements (overlaid in Fig. 6 as grey squares fit by a dashed black line). The data for both relaxation rates exhibit similar slopes but the T_2^{*-1} data are consistently offset from the T_2^{-1} data by around 1.5 s^{-1}. While our numerical results predict that T_2^{*-1} and T_2^{-1} should be approximately equal in these low-susceptibility materials, this offset implies that the dephasing rate is actually non-zero in the sands. The extent of dephasing, however, is sufficiently limited that it does not obscure the relationship between T_2^{*-1} and r_{grain}^{-1}. It is possible some unanticipated dephasing may result from residual magnetization of the grains following removal of the strong prepolarization field, or magnetic edge effects due to the finite sample volume. Such factors would be artefacts of the laboratory experimental design and are not expected to influence field NMR measurements in practice.

CONCLUSIONS

The numerical and laboratory experiments presented here provide insights into the link between T_2^* and geologic properties, needed to advance the use of surface NMR for hydrogeologic applica-

tions. Numerical models allow us to simulate the surface NMR relaxation response of geologic materials with widely varied pore size and magnetic susceptibility. These simulations illuminate the processes controlling T_2^* relaxation and identify restricted conditions in which hydrogeologically relevant information can be extracted from the T_2^* relaxation parameter. In geologic environments with low magnetic susceptibility, T_2^* is highly sensitive to variations in pore size, however, this sensitivity diminishes as susceptibility increases, particularly in coarser sediments. Complementary Earth's field NMR measurements support the numerical models and provide confirmation that, for weakly magnetic materials, T_2^* can provide a reliable indication of pore size and thus can potentially be used to estimate permeability.

In future work, it will be essential to consider the T_2^* response for a broader range of realistic geologic conditions. The numerical simulations presented here assume that magnetic properties of the grain do not vary within a sample. Improved numerical simulations will allow us next to consider the response of magnetically heterogeneous sediments. We will also extend our Earth's field laboratory experiments, which thus far have only considered low-susceptibility materials, to include a wider range of realistic geologic materials with higher magnetic susceptibility.

Our experiments here have only considered the effect of inhomogeneous fields arising due to magnetic grains. We note that in some locations, regional gradients in the magnetic field may significantly influence the T_2^* response, even when the aquifer sediments themselves are weakly magnetic. Finally, we point out that for the purposes of this study and in most previous studies, T_2^* relaxation has been treated as an exponential decay process. In actuality, our numerical simulations show that the FID can instead exhibit non-exponential decay under certain conditions. We are actively pursuing research to determine how the functional form of the FID may affect the interpretation of surface NMR measurements.

ACKNOWLEDGEMENTS

This material is based on work supported by the National Science Foundation under Grant No. EAR-0911234. Additional funding was received from British Petroleum, through a graduate research grant to E. Grunewald and from Schlumberger Water Services. We express our gratitude to Fairmount Minerals for donating the quartz sands used in the laboratory experiments. We would also like to thank the reviewers and editor for many helpful comments.

REFERENCES

Audoly B., Sen P.N., Ryu S. and Song Y.-Q. 2003. Correlation functions for inhomogeneous magnetic field in random media with application to a dense random pack of spheres. *Journal of Magnetic Resonance* **164**, 154–159.

Brownstein K.R. and Tarr C.E. 1979. Importance of classical diffusion in NMR studies of water in biological cells. *Physical Review A* **19**, 2446–2453.

Callaghan P.T., Coy A., Dykstra R., Eccles C.A., Halse M.E., Hunter M.W., Mercier O.R. and Robinson J.N. 2007. New Zealand developments in Earth's field NMR. *Applied Magnetic Resonance* **32**, 63–74.

Carr H.Y. and Purcell E.M. 1954. Effects of diffusion on free precession in nuclear magnetic resonance experiments. *Physical Review* **94**, 630–638.

Chen Q., Marble A.E., Colpitts B.G. and Balcom B.J. 2005. The internal magnetic field distribution, and single exponential magnetic resonance free induction decay, in rocks. *Journal of Magnetic Resonance* **175**, 300–308.

Dunn K.-J., Bergman D.J. and Latorraca G.A. 2002. *Nuclear Magnetic Resonance Petrophysical and Logging Applications*. Pergamon.

Gallegos D.P., Munn K. and Smith D. 1987. A NMR technique for the analysis of pore structure: Application to materials with well-defined pore structure. *Journal of Colloid and Interface Science* **119**, 127–140.

Hertrich M. 2008. Imaging of groundwater with nuclear magnetic resonance. *Progress in Nuclear Magnetic Resonance Spectroscopy* **53**, 227–248.

Hunt C.P., Moskowitz B.M. and Banerjee S.K. 1995. Magnetic properties of rocks and minerals. In: *Rock Physics and Phase Relations: A Handbook of Physical Constants* (ed. Thomas J. Ahrens), pp. 189–204. American Geophysical Union.

Hürlimann M.D. 1998. Effective gradients in porous media due to susceptibility differences. *Journal of Magnetic Resonance* **131**, 232–240.

Kenyon W.E., Howard J.J., Sezginer A., Straley C., Matteson A., Horkowitz K. and Ehrlich R. 1989. Pore-size distriubtuion and NMR in microporous cherty sandstones. SPWLA 13th Annual Logging Symposium, Expanded Abstracts, LL.

Kenyon W.E., Straley C. and Willemsen J.F. 1988. A three-part study of NMR longitudinal relaxation properties of water-saturated sandstones. *SPE Formation Evaluation* **3**, 622–636.

Legchenko A., Baltassat J.M., Beauce A. and Bernard J. 2002. Nuclear magnetic resonance as a geophysical tool for hydrogeologists. *Journal of Applied Geophysics* **50**, 21–46.

Legchenko A. and Valla P. 2002. A review of the basic principles for proton magnetic resonance sounding measurements. *Journal of Applied Geophysics* **50**, 3–19.

Lide D.R. 2003. *CRC Handbook of Chemistry and Physics*, 84th edn. CRC Press.

Lubczynski M. and Roy J. 2003. Hydrogeologic interpretation and potential of the new magnetic resonance sounding (MRS) method. *Journal of Hydrogeology* **283**, 19–40.

Mendelson K.S. 1993. Continuum and random-walk models of magnetic relaxation in porous media. *Physical Review B* **47**, 1081–1083.

Müller M., Kooman S. and Yaramanci U. 2005. Nuclear magnetic resonance (NMR) properties of unconsolidated sediments in field and laboratory. *Near Surface Geophysics* **3**, 275–285. doi:10.3997/1873-0604.2005023

Plata J. and Rubio F. 2008. The use of MRS in the determination of hydraulic transmissivity: The case of alluvial aquifers. *Journal of Applied Geophysics* **66**, 128–139.

Roy J., Rouleau A., Chouteau M. and Bureau M. 2008. Widespread occurrence of aquifers currently undetectable with the MRS technique in the Grenville geological province, Canada. *Journal of Applied Geophysics* **66**, 82–93.

Schirov M., Legchenko A. and Creer G. 1991. A new direct non-invasive groundwater detection technology for Australia. *Exploration Geophysics* **22**, 333–338.

Semenov A. 1987. NMR hydroscope for water prospecting. Proceedings of the Seminar on Geotomography, Hyderabad, Expanded Abstracts, 66–67.

Simpson J.H. and Carr H.Y. 1958. Diffusion and nuclear spin relaxation in water. *Physical Review* **111**, 1201–1202.

Song Y.-Q. 2003. Using internal magnetic fields to determine pore size distributions of porous media. *Concepts in Magnetic Resonance Part A* **18**, 97–110.

Straley C., Rossini D., Vinegar H.J., Tutunjian P.N. and Morriss C.E. 1997. Core analysis by low-field NMR. *The Log Analyst* **38**, 84–94.

Timur A. 1969. Pulsed nuclear magnetic resonance studies of porosity, movable fluid, and permeability of sandstones. *Journal of Petroleum Technology* **21**, 775–786.

Valckenborg R.M.E., Huinink H.P., v.d. Sande J.J. and Kopinga K. 2002. Random-walk simulations of NMR dephasing effects due to uniform magnetic-field gradients in a pore. *Physical Review E* **65**, 21306–21313.

Vouillamoz J.-M., Descloitres M., Bernard J., Fourcassier P. and Romagny L. 2002. Application of integrated magnetic resonance sounding and resistivity methods for borehole implementation. A case study in Cambodia. *Journal of Applied Geophysics* **50**, 67–81.

Walsh D.O. 2008. Multi-channel surface NMR instrumentation and software for 1D/2D groundwater investigations. *Journal of Applied Geophysics* **66**, 82–93.

Yaramanci U., Lange G. and Knoedel K. 1999. Surface NMR within a geophysical study of the aquifer at Haldensleben (Germany). *Geophysical Prospecting* **47**, 923–943. doi:10.1046/j.1365-2478.1999.00161.x